INELASTIC BEHAVIOUR OF REINFORCED CONCRETE MEMBERS WITH CYCLIC LOADING

D. C. Kent* and R. Park**

Summary

The results of an investigation into the behaviour of reinforced concrete members subjected to cyclic loading in the inelastic range are summarized. The investigation commences with studies of the Bauschinger effect for cyclically stressed mild steel reinforcement and the influence of rectangular steel hooping on the stress-strain behaviour of concrete. Using these derived stress-strain curves the moment-curvature relationships for reinforced concrete members under cyclic loading are studied theoretically and compared with the results of a series of tests on reinforced concrete beams under cyclic loading.

1. Introduction

The growing use of digital computers as a design tool has resulted in very rapid advances in the dynamic analyses of structures. However, the study of the factors on which such analyses are based, namely the behaviour of structural components, has fallen behind. This is well illustrated by the inaccurate elasto-plastic idealization for moment-rotation behaviour under cyclic loading which is generally used to predict the inelastic response of reinforced concrete structures subjected to seismic ground motions.

Most of the existing evidence concerning the post-elastic behaviour of reinforced concrete members has been obtained from theoretical work or tests in which the loads have been applied monotonically until failure. Few investigations have been conducted to determine the behaviour of reinforced concrete members under high intensity cyclic loading typical of seismic motions. Examples of investigations into the behaviour of reinforced concrete members under cyclic loading are those of Aoyama[1], Agrawal, Tulin and Gerstle[2], Burns and Seiss[3], Hanson and Conner[4] and Betero and Bresler[5]. Theoretical moment-curvature plots have been obtained by Agrawal, et al[2], on the basis of simplified stress-strain curves for the steel (including the Bauschinger effect) and the concrete, but many other investigators have ignored the Bauschinger effect and the majority of the work has been experimental.

This paper summarizes an investigation[6] which extends existing work. The investigation commences with studies of the Bauschinger effect for mild steel reinforcement and the stress-strain behaviour of concrete confined by steel hoops. On the basis of the derived stress-strain curves the moment-curvature relationships for reinforced concrete members under cyclic loading are studied theoretically and compared with test results.

* Programmer Analyst, Systems and Programmes Limited, Lower Hutt.
** Professor of Civil Engineering, University of Canterbury.

2. Stress-Strain Properties of Mild Steel

2.1 Stress of the Same Sign

The stress-strain relationship for mild steel subjected to monotonic loading is well known and easily defined. Fig. 1 shows this behaviour. Under repeated loading of the same sign the unloading and reloading stress-strain paths follow the initial elastic slope and when the strain regains the value at which unloading commenced the stress-strain curve continues as if unloading had not occurred. Hence the monotonic stress-strain curve forms an envelope for repeated loading regardless of whether unloading is initiated in the elastic, plastic or strain-hardening region. However this is not the case when the sign of the stress is reversed.

2.2 Reversal of Stress

Little information is available regarding the behaviour of reinforcing steel when subjected to alternating tensile and compressive stress. Under cyclic loading the stress-strain properties of steel become quite different from those associated with purely tensile or compressive stress. This is known as the Bauschinger effect and results in a lowering of the reversed yield stress. Once this phenomenon has been initiated by a yield excursion, linearity between stress and strain is lost over much of the loading range. This steel behaviour is strongly influenced by previous strain history; time and temperature also have an effect. Fig. 2 illustrates the properties of the Bauschinger effect. It should be noted that the unloading path of both signs follows the initial elastic slope, as does the reloading path, after which the stress-strain curve resumes as if unloading had not occurred. This is of importance because it means that in a structure after an earthquake there will not be incremental failure in the steel due to repeated live loading. The reversed stress at which the Bauschinger effect commences, but below which the Bauschinger effect does not occur, is known as the transition stress.

In a preliminary study of the Bauschinger effect Singh, Gerstle and Tulin[7] found that the history of previous loading had an effect on the slope of the curved part of the reversed stress-strain curve. Nevertheless, from their experiments they arrived at a simple expression representing an average of the family of

reversed loading curves. Their expression

$$f_s = 64,500 - 52,700\,(0.838)^{1000\varepsilon_s} \text{ p.s.i.} \quad \ldots (1)$$

represents a curve which is extended backwards to meet an initial elastic slope at the transition stress as is shown in Fig. 3. The test specimens on which equation (1) was based all came from the same batch and hence variations in the virgin properties of the steel were not considered in their investigation.

2.3 Cyclic Loading Tests on Steel Specimens

To check the validity of equation (1) for a variety of mild steel bars and to examine other possible mathematical representations for the Bauschinger effect a number of New Zealand rolled deformed bar specimens of $\frac{1}{2}$", $\frac{5}{8}$", $\frac{3}{4}$" and $\frac{7}{8}$" diameter were tested[6]. The variables studied were the virgin properties of the material and the previous strain history. The loading was applied statically but Singh, et al[7], have reported that the effect of rate of straining is not noticeable over the usual range of test speeds. Hence the results should be applicable to the strain rates associated with seismic loading.

The test specimens were $5\frac{1}{4}$" long between the end plates. The central $2\frac{2}{4}$" length was machined to $\frac{1}{4}$" diameter for the $\frac{1}{2}$" and $\frac{5}{8}$" diameter bars and to $\frac{1}{2}$" diameter for the $\frac{3}{4}$" and $\frac{7}{8}$" diameter bars. The specimens were screwed into the end plates and bolted into a specially constructed test rig. The load was applied by means of screw jacks as their use allowed strain control when loading in the plastic range. The strain was measured over a 2" gauge length. Considerable care was taken to ensure that eccentric loading did not become significant during the loading runs. However slight eccentricity of loading may have been present because the yield stresses measured were consistently 3000 - 5000 p.s.i. lower than those obtained from machined specimens of the same bar tested in an Avery testing machine, and the yield point was not so distinct. The ultimate stresses by comparison were almost identical. A variety of loading cycles was applied to study a range of initial strains and unloading and reloading sequences from tension and compression after the Bauschinger effect had been initiated.

2.4 Further Expression for Bauschinger Effect

To determine a general formula for the loading (curved) part of the stress-strain curve, each cycle of eleven test specimens was isolated and subjected to a least squares analysis for a variety of possible mathematical expressions[6]. Firstly, the Singh, et al, equation (1) was generalized by putting the yield and ultimate stresses in the numeral constants in general terms. However, unsatisfactory correlation was obtained with previous strain history; in particular the calculated transition stress was too high. A variety of other mathematical formulations were also tried and found to be unsatisfactory.

Finally the Ramberg-Osgood function was chosen. This function can be written in terms of stress and strain as follows :

$$\frac{\varepsilon_s}{\varepsilon_{ch}} = \frac{f_s}{f_{ch}}\left(1 + \left|\frac{f_s}{f_{ch}}\right|^{r-1}\right) \quad \ldots (2)$$

where ε_{ch} and f_{ch} are the "characteristic" strain and stress, respectively, and r is the Ramberg-Osgood parameter. Fig. 4 shows a plot of equation (2). The shape of the curve changes with the value of r. Inspection shows f_{ch} and ε_{ch} are related such that

$$f_{ch} = E_s \varepsilon_{ch} \quad \ldots (3)$$

Hence given E_s the function simplifies to an equation involving two unknowns, r and f_{ch}. A disadvantage of equation (2), however, is that an increase in strain will always result in an increase in stress and the desirable boundary conditions of $df_s/d\varepsilon_s = o$ and $f_s = f_{su}$ when $\varepsilon_s = \varepsilon_{su}$ cannot be complied with. Hence the expression can only be expected to apply accurately when $\varepsilon_s << \varepsilon_{su}$.

The values for f_{ch} and r for each of the loading cycles of the eleven test specimens were determined using a least squares analysis. It was found that the ratio f_{ch}/f_y was dependent on the amount of plastic strain produced in the previous cycle ε_{ipl}, the ratio f_{ch}/f_y becoming lower with increasing prior plastic strain. With the help of a least squares analysis the following equation for f_{ch} was fitted:

$$f_{ch}/f_y = \frac{0.744}{\log_e(1+1000\varepsilon_{ipl})} + \frac{0.071}{(e^{1000\varepsilon_{ipl_{-1}}})} + 0.241 \quad \ldots (4)$$

Equation (4) gives $f_{ch}/f_y < 1$ when $\varepsilon_{ipl} > 0.0015$, reducing to 0.45 when $\varepsilon_{ipl} = 0.022$.

When the values for r given by equation (4) were plotted against the various factors only the cycle number N showed any correlation with r. The cycles were numbered N = 0, 1, 2, ... where first yield occurs at a cycle number N = 0 and N = 1 is the first post-yield stress reversal. There was a good deal of scatter in the plotted results but the odd-numbered cycles showed lower values of r than the even-numbered cycles, and r became smaller as N increased. A least squares analysis gave the following expressions for r:

For odd-numbered cycles:

$$r = \frac{4.49}{\log_e(1+N)} - \frac{6.03}{e^N - 1} + 0.297 \quad \ldots (5)$$

For even-numbered cycles:

$$r = \frac{2.20}{\log_e(1+N)} - \frac{0.469}{e^N - 1} + 3.04 \quad \ldots (6)$$

In the first eight cycles, the value for r given by equations (5) and (6) was between 4 and 5 for N even and between $2\frac{1}{2}$ and $3\frac{1}{2}$ for N odd.

It is to be noted that equations (2) to (6) apply to the loading parts of the stress-

strain curve. The unloading parts are straight lines parallel to the initial elastic slope.

Figs. 5 and 6 show the experimental points measured for two of the test specimens compared with the stress-strain curves calculated from the modified Ramberg-Osgood function, equations (2) to (6), and the Singh, et al, expression, equation (1). In all but two of the eleven specimens the modified Ramberg-Osgood function was more accurate than the Singh, et al, expression. For cycles of large strain range the Singh, et al, expression tends to be less inaccurate but in cycles of lower strain range the modified Ramberg-Osgood function is clearly better.

3. Stress-Strain Properties of Concrete

The properties of the compressive stress block for a flexural member depend on the shape of the stress-strain curve for the concrete.

3.1 Unconfined Concrete With Monotonic Loading

Probably the most widely accepted idealization for the stress-strain curve of concrete compressed in one direction is that due to Hognestad[8] which consists of a second degree parabola up to maximum stress and then a linear falling branch. More recent work by Hognestad, Hanson and McHenry[9] determined the compressive stress block parameters directly from tests on eccentrically loaded specimens which simulated the compression zone of a flexural member and found a striking similarity between the stress-strain curves determined from their eccentrically loaded specimens and concentrically loaded cylinders. This is in contrast with the tests of Sturman, Shah and Winter[10] which indicated that a strain gradient caused an increase in maximum stress and an increase in the strain at maximum stress. An important property of concrete which has been observed in all tests is that at loads approaching the maximum the concrete actually increases in volume as it undergoes progressive internal fracturing.

3.2 Confined Concrete With Monotonic Loading

In practice concrete may be confined by transverse reinforcement in the form of closely spaced steel hoops or spirals. The concrete becomes confined when at stresses approaching the uniaxial strength it commences to increase in volume and bears out against the transverse reinforcement which then applies a confining reaction to the concrete. Rectangular hoops do not confine the concrete as effectively as circular spirals because the confining reaction can only be applied to the corner regions of the section since the bending resistance of the transverse steel between the corners is insufficient to restrain the expansion of the concrete along the sides, as is illustrated in Fig. 7. Roy and Sozen[11] did not observe any increase in concrete strength due to the presence of square hoops, but other investigators, for example Stöckl[12] and Betero and Felippa[13], have observed a small increase. Nevertheless, there is general agreement that rectangular hoops do produce a significant increase in the ductility of the concrete core as a whole.

On the basis of existing experimental evidence it is proposed[6] that the curve shown in Fig. 8 gives a good representation for the stress-strain curve for concrete in compression. The various regions are:

Region OA: The ascending portion of the curve will be represented by a second degree parabola with a maximum stress equal to the cylinder strength f'_c at a strain of 0.002. This maximum stress ignores any small increase in strength that may occur due to strain gradient or confinement and any small reduction that may occur in beams without any confinement. It is commonly accepted that the strain at maximum stress is 0.002. Hence for region OA

$$f_c = f'_c \left(\frac{2\varepsilon_c}{\varepsilon_o} - \left(\frac{\varepsilon_c}{\varepsilon_o}\right)^2 \right) \qquad \ldots (7)$$

where $\varepsilon_o = 0.002$

Region AB: The falling branch of the curve will be assumed to be linear and its slope will be specified by determining the strain when the stress is $0.5f'_c$. Examination of the test results of a number of investigators shows that for unconfined concrete the strain at $0.5f'_c$ on the falling branch for short-term loading rates can be represented reasonably well by the expression (with f'_c in p.s.i.) :-

$$\varepsilon_{50u} = \frac{3 + 0.002f'_c}{f'_c - 1000} \qquad \ldots (8)$$

This relationship shows that high strength concretes have considerably lower ε_{50u} values, i.e. they are more brittle.

For concrete confined by rectangular hoops the slope of the falling branch is reduced. One variable effecting the slope is the volumetic ratio of confining steel

$$p'' = \frac{2(b'' + d'')A''_s}{b''d''s} \qquad \ldots (9)$$

Another is the ratio of hoop spacing to minimum core dimension, s/b'', because clearly the confinement of the concrete between the hoops depends on the arching action between the hoops and if the s/b'' ratio is large a considerable volume of concrete will spall away as is illustrated in Fig. 9. Since the core area of confined concrete will be considered as that area within the outside dimensions of the hoops it is clear that a large s/b'' ratio will lead to a smaller mean stress over the core area for the same p'' value. The hoop yield stress will not be taken as a variable because there is no guarantee that the hoops will reach that stress.

A measure of the additional strain at $0.5f'_c$ on the falling branch due to confinement is given by

$$\varepsilon_{50h} = \varepsilon_{50c} - \varepsilon_{50u} \qquad \ldots (10)$$

Values for ε_{50h} were found from equation (10) using values for ε_{50c} scaled off previously published experiental stress-strain curves for confined concrete[11, 13, 14] and the values for ε_{50u} calculated from equation (8). The relationship between the values for ε_{50h} so found and the corresponding p'' and b''/s ratios were next examined by a least squares analysis.

There was considerable scatter of the test results. The relationship finally chosen was:

$$\varepsilon_{50h} = \frac{3}{4} p'' \sqrt{\frac{b''}{s}} \quad \ldots (11)$$

Equation (11) and Fig. 8 indicate that there is a great improvement in the falling branch behaviour for small contents of hoops, but that the improvement becomes progressively less significant as more hoops are added. Examination of the coordinates of line AB of Fig. 8 shows that the equation for AB may be written as

$$f_c = f'_c \{1 - Z (\varepsilon_c - \varepsilon_o)\} \quad \ldots (12)$$

$$\text{where } Z = \frac{0.5}{\varepsilon_{50h} + \varepsilon_{50u} - \varepsilon_o} \quad \ldots (13)$$

$\varepsilon_o = 0.002$ and ε_{50h} and ε_{50u} are given by equations (11) and (8), respectively. It is to be noted that Z decreases as the volumetric ratio p" increases.

Region BC: It will be assumed that the concrete can sustain a stress of $0.2f'_c$ at strains greater than ε_{20c}. This assumption has been made previously by Yamashiro and Seiss[15].

3.3 Modulus of Rupture for Monotonic Loading

A linear stress-strain curve for concrete in tension (region OD of Fig. 8) is assumed with the same slope as the curve for compression at zero stress. The maximum tensile stress will be taken as that proposed by Warwaruk[16] (with f'_c in p.s.i.):

$$f'_t = \frac{1000 f'_c}{4000 + f'_c} \text{ p.s.i.} \quad \ldots (14)$$

3.4 Cyclic and Repeated Loading of Concrete

Fig. 10 shows the effect of repeated loading on concrete. The idealized repeated and cyclic loading response illustrated in the figure will be assumed. On unloading from point A it is assumed that 75% of the previous stress is lost without decrease in strain and then a linear path of slope $0.25E_c$ is followed to point C. If the concrete has not cracked it is capable of carrying tensile stress to point G, but if the concrete has previously cracked or cracks form during this loading stage the tensile strains increase without any tensile stress developing. On reloading the strain must regain the value at C before compressive stress can be sustained again. If reloading commences before unloading produces zero compressive stress then reloading follows one of the paths EF. It is to be noted that the average slope of the assumed loop between A and C is parallel to the initial tangent modulus of the stress-strain curve. It is thought that more complicated idealization of the loop would be unwarranted.

4. Theoretical Moment—Curvature Response for Cyclically Loaded Reinforced Concrete Sections

4.1 Basic Assumptions

To determine the moment-curvature characteristics of reinforced concrete sections with cyclic loading the following assumptions will be made:

(i) The longitudinal strain in the steel and concrete at the various levels is directly proportional to distance from the neutral axis.
(ii) The stress-strain curve for the steel reinforcement under cyclic loading is as given by the equations of Section 2.4.
(iii) The stress-strain characteristics for the concrete under cyclic loading is as assumed in Section 3.4 and by the equations of Sections 3.2 and 3.3, but that unconfined compressed concrete carries no stress at strains greater than 0.004.

The first assumption is normally made in reinforced concrete theory. The second assumption means that the Bauschinger effect will be taken into account. It should be noted however that the possibility of buckling of the compression steel is ignored. The third assumption means that the cover concrete has the same stress-strain curve as the confined core at compressive strains of less than 0.004 but at greater strains the cover concrete spalls and does not carry stress. It is difficult to determine accurately the spalling strain of the cover concrete. The assumption may appear to be conservative but it has been observed that the presence of a high quantity of steel hooping tends to precipitate spalling[17]. Also, it is felt that the cover concrete would soon become ineffective after several reversals of high intensity loading. It should also be noted that it is assumed that the proposed stress-strain curve for confined concrete applies regardless of the position of the neutral axis within the hoops although this curve was derived from tests in which all the concrete was compressed. This is considered reasonable because of the helpful confining effect of the higher strain gradient and the presence of the lowly stressed concrete beneath the neutral axis.

4.2 Method of Solution

Computer programs were developed[6] to compute the bending moment and curvature for cyclically loaded reinforced concrete T or rectangular sections with or without constant axial compression. The programs operate within stipulated curvature cycles. The approach adopted was to divide the concrete section into a number of discrete elements. Each element has the width of the section at that level; if there are n elements each will have depth h/n. Fig. 11 shows the arrangement for a T section. The top and bottom steel reside in elements nd'/h and nd/h, respectively. If the strain in the top fibre is ε_{cm} and the neutral axis depth is kd then the average strain in element i is given as

$$\varepsilon_i = \varepsilon_{cm} \frac{n\frac{kd}{h} - i + 0.5}{n\frac{kd}{h}} \quad \ldots (15)$$

The stress in each concrete element or steel bar is taken as that corresponding to the average strain in the element. From the stresses and the areas of the elements or bars the forces on the section may be determined.

An iterative technique is used to calculate points on the moment-curvature curves. The strain ε_{cm} in the top concrete fibre is adjusted by a fixed amount. For each value of ε_{cm}, the neutral axis depth kd is estimated and stresses in the elements computed for this strain profile. The forces acting on the elements are then calculated and the equilibrium of the forces checked using the requirement that

$$\Sigma C - \Sigma T = P \qquad \ldots (16)$$

where C and T are the compressive and tensile forces acting on the elements, respectively, and P is the compressive load acting on the section (zero in the case of a beam). If the equilibrium equation (16) is not satisfied the estimated neutral axis position is incorrect and is adjusted until equilibrium of forces is achieved. Having obtained equilibrium the bending moment and curvature are calculated for the particular ε_{cm} value.

The discrete element technique has the advantage of coping with unusual stress distributions and it is a simple matter to alter the element force for area reductions due to spalling and to record which elements have cracked. The technique has the disadvantage of being relatively slow in that it is necessary to store for each element the parameters that record the progress along the stress-strain path in order to calculate the stress corresponding to a given strain.

Using the analysis outlined above, approximately 60 minutes of IBM 360/44 computer time was necessary to produce the moment-curvature responses for 14 or 15 cycles using an ε_{cm} increment of 0.0001 for each of the beam sections described in Section 5.

5. Experimental Moment—Curvature Response

To assess the accuracy of the theoretical approach of Section 4 a series of reinforced concrete beams were tested under cyclic loading. Each beam was supported over a span of 9 ft. between pins which allowed free rotation and horizontal translation at the supports. All beams had a rectangular section $4\frac{15}{16}$" wide x 8" deep and were cast with a 20" high x 8" long x $4\frac{15}{16}$" wide column stub at mid-span. Deformed steel bars with a yield stress in the range 45,700 to 49,200 p.s.i. were used as longitudinal reinforcement. Each beam contained two bars of $\frac{1}{2}$" diameter in the top (1.1% of steel) and two bars of either $\frac{1}{2}$" or $\frac{5}{8}$" or $\frac{3}{4}$" or $\frac{7}{8}$" diameter in the bottom (1.1% or 1.8% or 2.5% or 3.5% of steel); the cover to this steel was 1". The stirrups were of $\frac{1}{4}$" diameter plain mild steel bar at either 2" or 4" or 6" spacing, giving p" as either 2.3% or 1.2% or 0.77%. At the time of testing the concrete cylinder strength was in the range 4650 to 7490 p.s.i.

Each beam was loaded statically at mid span by means of screw jacks applied to the top and bottom of the column stub. Screw jacks rather than hydraulic jacks were used to obtain deflection control in the plastic range. Generally the loading consisted of several cycles to design load, several cycles in the inelastic range, several cycles to design load and then a cycle to failure. To allow strain measurements on the longitudinal bars, $\frac{1}{4}$" diameter by 1" long steel lugs were welded on to the longitudinal bars and protruded sideways out through enlarged holes in the cover concrete. This allowed longitudinal steel strain readings to be taken by placing a Demec strain gauge between the ends of the lugs. Fig. 12 shows a beam after testing.

The experimental curvature was calculated from the measured strains in the compression and tension steel over a 2in. gauge length in the beam adjacent to the column stub. Figs. 13, 14 and 15 show the experimental moment-curvature characteristics measured at the critical section of some of the test beams. Lines rather than points illustrate the experimental curvatures in the figures, reflecting the creep which occurred during each increment. In the figures positive bending moment arises from downward load on the beams and positive curvature corresponds to tension on the bottom of the beam.

6. Discussion of Moment—Curvature Response

The theoretical moment-curvature responses for the sections calculated between the experimental curvature points at which moment reversal took place are shown plotted in Figs. 13, 14 and 15.

Notable features of these curves are as follows :

(i) Over a large proportion of the theoretical curves the moment is carried by a steel couple alone. This phenomenon is due to yielding of the steel in tension causing cracks in the tension zone which, because of plastic elongation of the steel, do not close when the moment is returned to zero. When the direction of moment is changed that steel is put into compression and must carry all the compressive force because cracks now exist in the compression zone. The steel must yield in compression before these cracks close and enable some of the compressive force to be carried by the concrete. Thus the concrete may not carry compression over large portions of the moment-curvature response to cyclic loading. This is well illustrated in Figs. 13, 14 and 15.

(ii) The flexural stiffness of the section is reduced when the moment is being carried by steel couple alone but increases when the concrete commences to carry compression. The increase in stiffness due to closing of the cracks in the compression zone is more sudden in the theoretical curves than in the tests, as is shown in Figs. 14 and 15. This is probably because in practice clean cracks do not occur. Particles of concrete which flake off during cracking and small relative shear displacements along the cracks cause compression to be transferred across the cracks gradually as high spots come into contact rather than suddenly as is implied in the theory.

(iii) The curved nature of the moment-curvature curves after the first yield excursion is due to the Bauschinger effect of the steel. The beam of Fig. 13 had equal top and bottom steel and after the first yield excursion the load is carried very largely by the steel couple and therefore the shape of the moment-curvature loop is very much governed by the shape of the stress-strain loop for the steel.

(iv) For the beam of Fig. 13 with equal

top and bottom steel the high theoretical moment carrying capacity in the final cycle to failure is due to the Ramberg-Osgood expression giving a high theoretical steel stress at large strains. For the beam of Fig. 15 with a relatively small top steel area and large hoop spacing the theoretical moment is low in the final cycle to failure. One reason for this is that the load carried by the cover concrete is ignored at compressive strains greater than 0.004 and evidently not all of this concrete was lost. In these beams the ratio of core width to total width had the low value of 0.70. For higher and more realistic values for this ratio the discrepancy in moment would become much smaller.

(v) It is evident that both the theoretical and experimental curves are far removed from the classical elasto-plastic shape. A better idealization for their shape would be a Ramberg-Osgood shaped response illustrated in Fig. 16 or the degrading stiffness response suggested by Clough[18] shown in Fig. 17. The idealization of Fig. 16 would be especially applicable to beams with approximately equal top and bottom steel areas, and that of Fig. 17 would be more applicable to beams with different top and bottom steel areas.

(vi) There are stages in the loading cycles when open cracks exist down the full depth of the member. One implication of this is that the ability of the concrete to carry shear force could be severely impaired and splitting along the longitudinal bars may occur due to the dowel forces. The nominal shear stress in the test beams at ultimate load varied between 120 p.s.i. for the beams with $\frac{1}{2}$" diameter tension steel and 350 p.s.i. for the beams with $\frac{7}{8}$" diameter tension steel. Based on a yield stress of 45,000 p.s.i., the stirrups were capable of carrying 150 p.s.i. of this shear stress when spaced at 6" centres and 450 p.s.i. when spaced at 2" centres. The ACI code value for the shear stress carried by the concrete, $2\sqrt{f'_c}$, varied between 140 and 170 p.s.i. for the beams. Thus it could be expected that after cyclic loading the beams carrying the highest shear force and with hoops spaced at 6" centres may have shown signs of distress in shear. This was not the case however, since all beams reached the ultimate flexural strength. However it is to be noted that the beams carrying the highest shear force (with $\frac{7}{8}$" diameter tension steel and $\frac{1}{2}$" diameter compression steel) did not have open cracks in the compression zone near ultimate moment. The worst case for shear transfer by the concrete would have been in the beams with equal top and bottom steel ($\frac{1}{2}$" diameter bars), since those beams had open cracks in the compression zone near ultimate moment, but because they had a smaller moment capacity they were not subjected to such a high shear force. The effect of cyclic loading on the shear capacity of beams requires further examination.

7. Conclusions

(i) The stress-strain properties of steel reinforcement after the first yield excursion cannot be accurately represented by an elasto-plastic model because of the Bauschinger effect. The Ramberg-Osgood function gives a good representation of the actual behaviour except at extremely high strains. The constants in the function were found to depend on the strain in the previous cycle and the number of previous cycles.

(ii) The confinement of compressed concrete by rectangular hoops leads to an improvement in the falling branch characteristics of the stress-strain curve for concrete which can be written as a function of the volumetric ratio of hoops and the ratio of hoop spacing to core width. The cyclic load behaviour of concrete can be represented by a series of straight lines.

(iii) The moment-curvature response of reinforced concrete beams with cyclic loading can be derived using the proposed stress-strain curves for steel and concrete. The theoretical curves compare reasonably well with experiment and illustrate the variation in stiffness due to the opening and closing of cracks in the compression zone of the concrete and the Bauschinger effect of the steel. For large portions of the moment-curvature curve after first yield open cracks exist in the compression zone and the moment of resistance is provided by the steel couple. During this part of the cyclic loading the main role of the concrete is to prevent the steel from buckling and the capacity of the concrete for carrying shear force may be reduced.

(iv) A great deal of computer time is involved in obtaining the theoretical moment-curvature responses for cyclic loading. It is suggested that a reasonably accurate idealization such as that illustrated in Figs. 16 or 17 could be used for the dynamic analysis of reinforced concrete structures rather than the inaccurate elasto-plastic idealization.

Acknowledgements

This work was carried out in the Department of Civil Engineering of the University of Canterbury by the first named author during postgraduate studies supervised by the second named author. The financial assistance of the University Grants Committee is gratefully acknowledged.

References

1. Aoyama, H., "Moment-Curvature Characteristics of Reinforced Concrete Members Subjected to Axial Load and Reversal of Bending", Proceedings of International Symposium on the Flexural Mechanics of Reinforced Concrete, ASCE-ACI, Miami, Fla., 1964.
2. Agrawal, G. L., Tulin, L. G. and Gerstle, K. H., "Response of Doubly Reinforced Concrete Beams to Cyclic Loading", Journal ACI, Proc. Vol. 62, No. 7, July 1965.
3. Burns, N. H. and Seiss, C. P., "Repeated and Reversed Loading in Reinforced Concrete", Journal of Structural Division, ASCE, Vol. 92, No. ST5, October 1966.
4. Hanson, N. W. and Conner, H. W., "Seismic Resistance of Reinforced Concrete Beam-Column Joints", Journal of Structural Division, ASCE, Vol. 93, No. ST5, October 1967.
5. Betero, V. V. and Bresler, B., "Seismic Behaviour of Reinforced Concrete Framed Structures", Fourth World Conference on Earthquake Engineering, Chile, 1969.
6. Kent, D. C., "Inelastic Behaviour of Reinforced Concrete Members with Cyclic Loading", Ph.D. Thesis, University of Canterbury, New Zealand, 1969.

7. Singh, A., Gerstle, K. H. and Tulin, L. G., "The Behaviour of Reinforcing Steel Under Reversed Loading", Journal ASTM, Materials Research and Standards, Vol. 5, No. 1, Jan. 1965.
8. Hognestad, E., "A Study of Combined Bending and Axial Load in Reinforced Concrete Members", University of Illinois Engineering Experimental Station, Bulletin No. 399, 1951.
9. Hognestad, E., Hanson, N. W. and McHenry, D., "Concrete Stress Distribution in Ultimate Strength Design", Journal ACI, Proc. Vol. 52, No. 4, December, 1955.
10. Sturman, G. M., Shah, S. P. and Winter, G., "Effects of Flexural Strain Gradients on Microcracking and Stress-Strain Behaviour of Concrete", Journal ACI, Proc. Vol. 62, No. 7, July, 1965.
11. Roy, H.E.H. and Sozen, M. A., "Ductility of Concrete", Proceedings of the International Symposium on Flexural Mechanics of Reinforced Concrete, ASCE-ACI, Miami, Fla., 1964.
12. Stöckl, S., Discussion on Reference 11.
13. Betero, V. V. and Felippa, C., Discussion on Reference 11.
14. Soliman, M.T.M. and Yu, C. W., "The Flexural Stress-Strain Relationship of Concrete Confined by Rectangular Transverse Reinforcement", Magazine of Concrete Research, Vol. 19, No. 61, December 1967.
15. Yamashiro, R. and Seiss, C. P., "Moment-Rotation Characteristics of Reinforced Concrete Members Subjected to Bending, Shear and Axial Load", Civil Engineering Studies, Structural Research Series No. 260, University of Illinois, December 1962.
16. Warwaruk, J., "Strength in Flexure of Bonded and Unbonded Prestressed Concrete Beams", Civil Engineering Studies, Structural Research Series No. 138, University of Illinois, August 1967.
17. Blakeley, R. W. G., and Park R., "Seismic Resistance of Prestressed Concrete Beam-Column Assemblies", Submitted to Journal of American Concrete Institute.
18. Clough, R. W., "Effect of Stiffness Degradation on Earthquake Ductility Requirements", Report No. 66-16, Structural Engineering Laboratory, University of California, October 1966.

Notation

A''_s	area of one leg of steel hoop
b''	width of confined core measured to outside of hoops
C	compressive force acting on concrete element or steel bar
d	distance to centroid of tension steel from extreme compression fibre
d'	distance to centroid of compression steel from extreme compression fibre
d"	depth of confined core measured to outside of hoops
E_c	tangent modulus of elasticity of concrete at zero stress
E_s	modulus of elasticity of steel
f_c	concrete stress
f'_c	strength of a 6" diameter x 12" concrete cylinder
f_{ch}	characteristic stress of steel in Ramberg-Osgood function
f_s	steel stress
f_{su}	ultimate steel stress
f'_t	modulus of rupture of concrete
	yield stress of steel
h	overall depth of section
i	element number
k	distance from neutral axis to extreme compression fibre/d
n	number of elements
N	cycle number
p	area of bottom steel/bd
p'	area of top steel/bd
p"	volume of steel hoops/volume of concrete core
P	axial load
r	Ramberg-Osgood parameter
s	spacing of hoops
T	tensile force acting on concrete element or steel bar
Z	defined by equation (13)
ε_c	strain in concrete
ε_{ch}	characteristic strain in steel of Ramberg-Osgood function
ε_{cm}	concrete strain at extreme compression fibre
ε_i	Average strain at element i
ε_{ipl}	plastic strain in steel produced in previous cycle
ε_o	concrete strain at maximum stress (0.002)
ε_s	steel strain
ε_{sh}	steel strain at commencement of strain hardening
ε_{su}	steel strain at ultimate steel stress
ε_{20c}	strain at 0.2 of maximum stress on falling branch of stress-strain curve for confined concrete
ε_{50c}	strain at 0.5 of maximum stress on falling branch of stress-strain curve for confined concrete
ε_{50h}	$\varepsilon_{50c} - \varepsilon_{50u}$
ε_{50u}	strain at 0.5 of maximum stress on falling branch of stress-strain curve for unconfined concrete

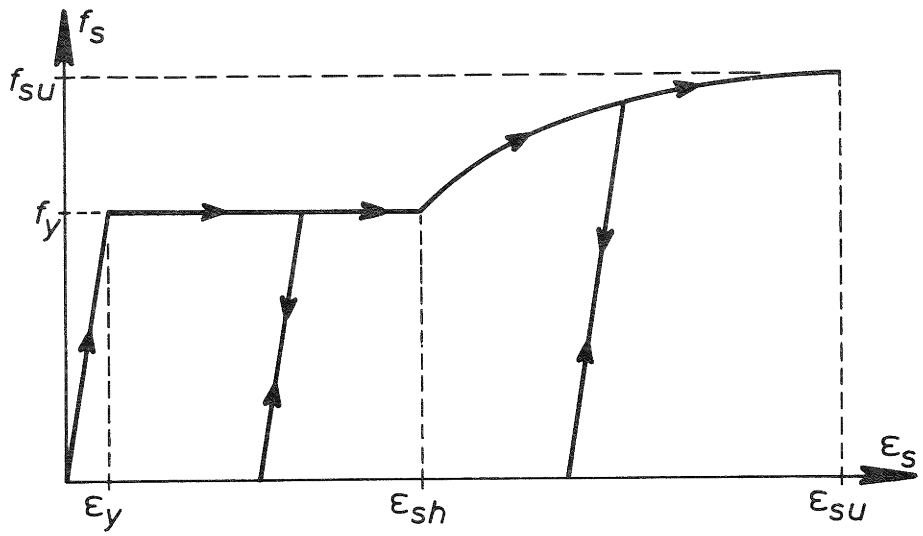
f_s
f_{su}
f_y
ε_s
ε_y
ε_{sh}
ε_{su}

Fig. 1

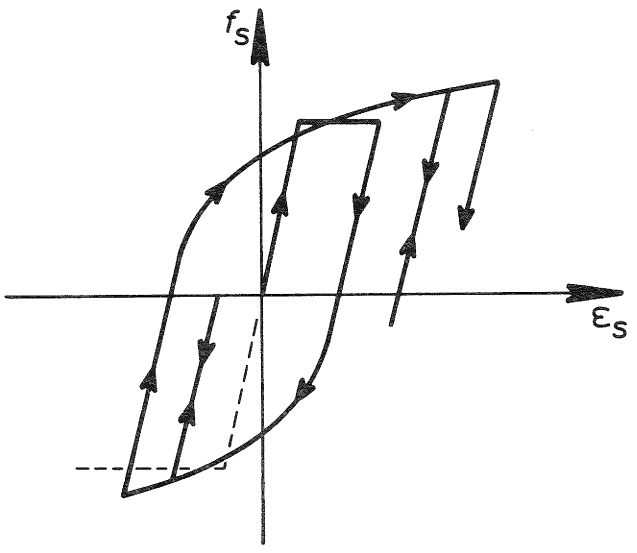
f_s
ε_s

Fig. 2

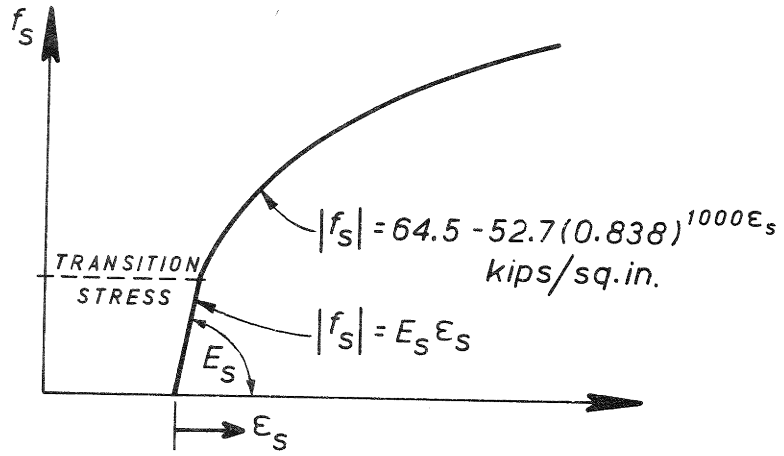
f_s
$|f_s| = 64.5 - 52.7(0.838)^{1000\varepsilon_s}$
kips/sq.in.
TRANSITION STRESS
$|f_s| = E_s\varepsilon_s$
E_s
ε_s

Fig. 3

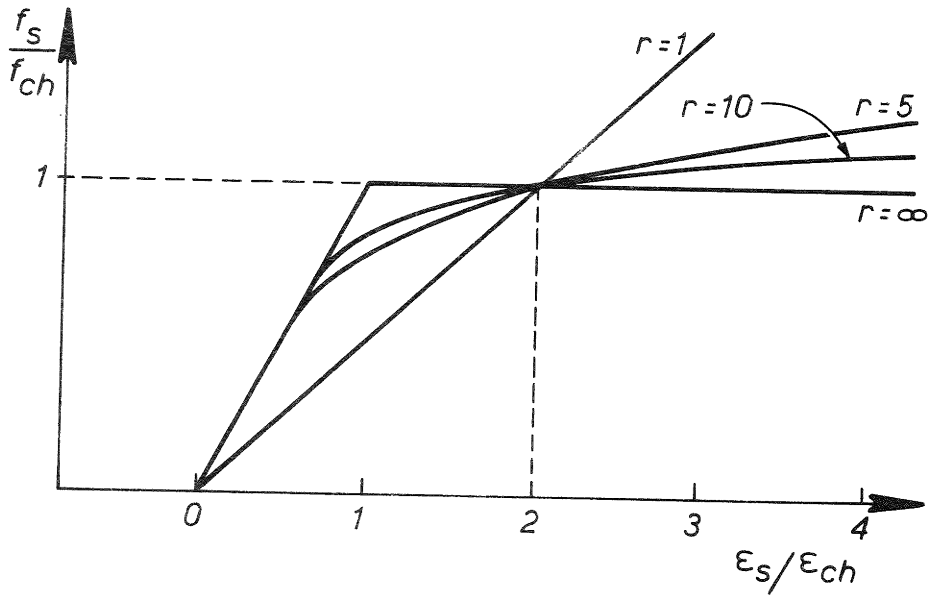
$\frac{f_s}{f_{ch}}$
1
r=1
r=10
r=5
r=∞
0
1
2
3
4
$\varepsilon_s/\varepsilon_{ch}$

Fig. 4

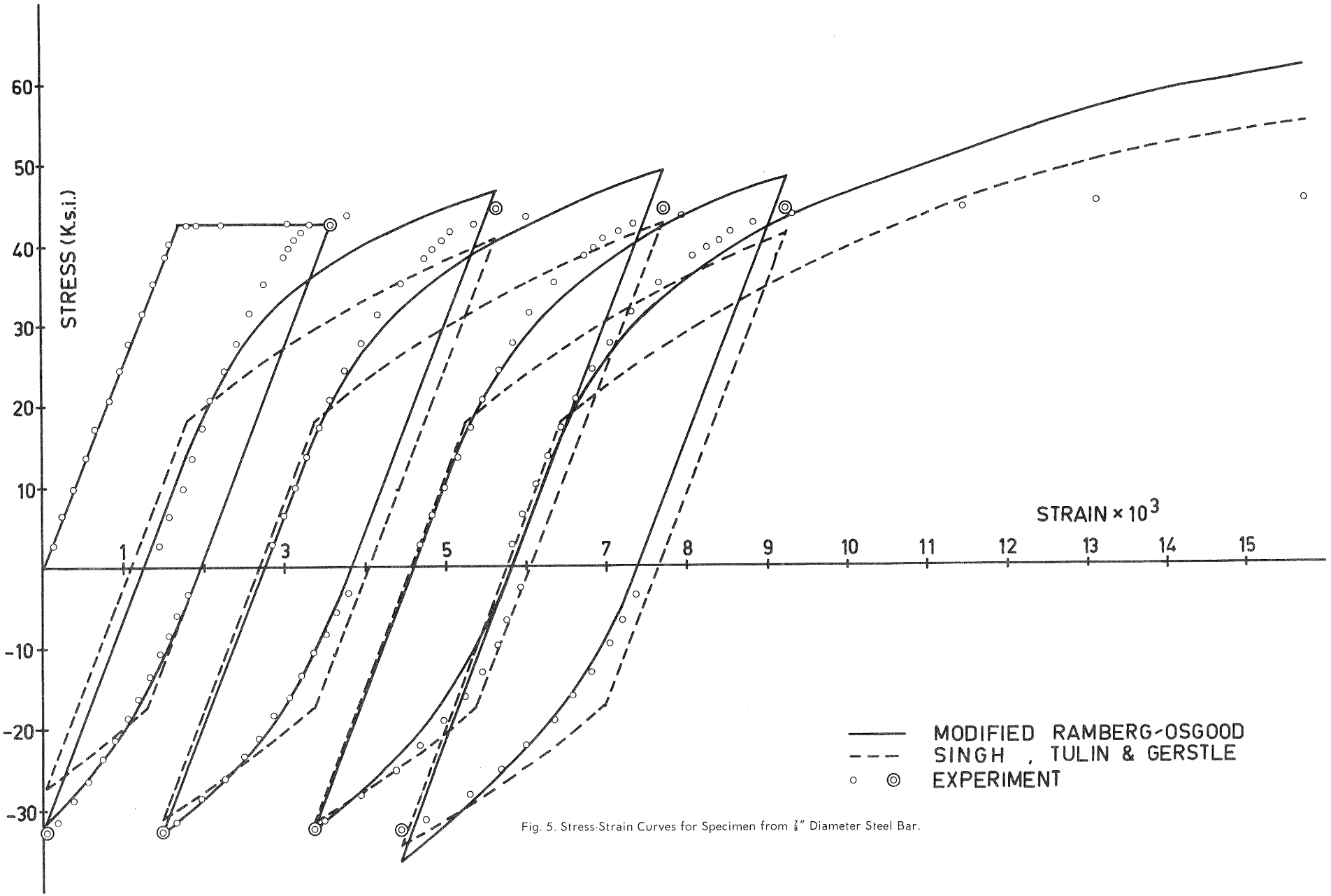

Fig. 5. Stress-Strain Curves for Specimen from $\frac{7}{8}$" Diameter Steel Bar.

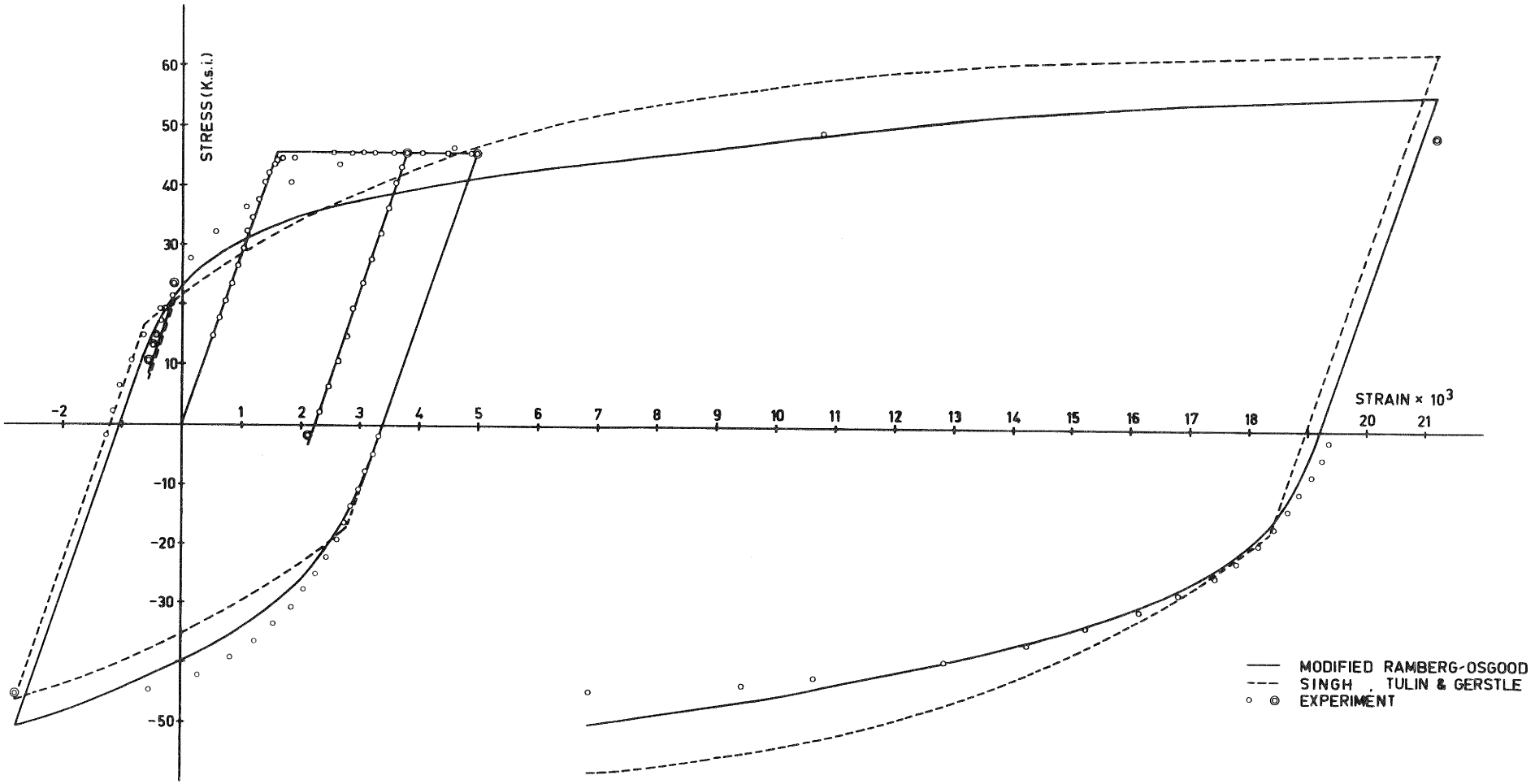

Fig. 6. Stress-Strain Curves for Specmen from $\frac{1}{2}$" Diameter Steel Bar.

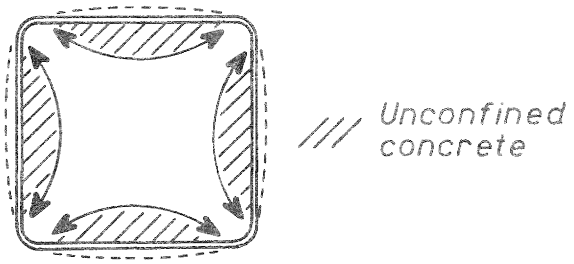

Fig. 7

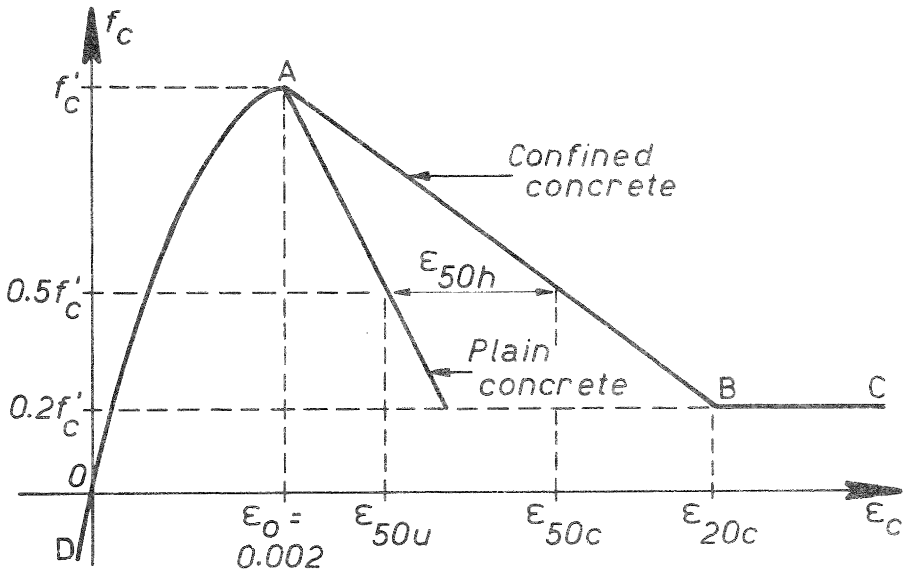

Fig. 8

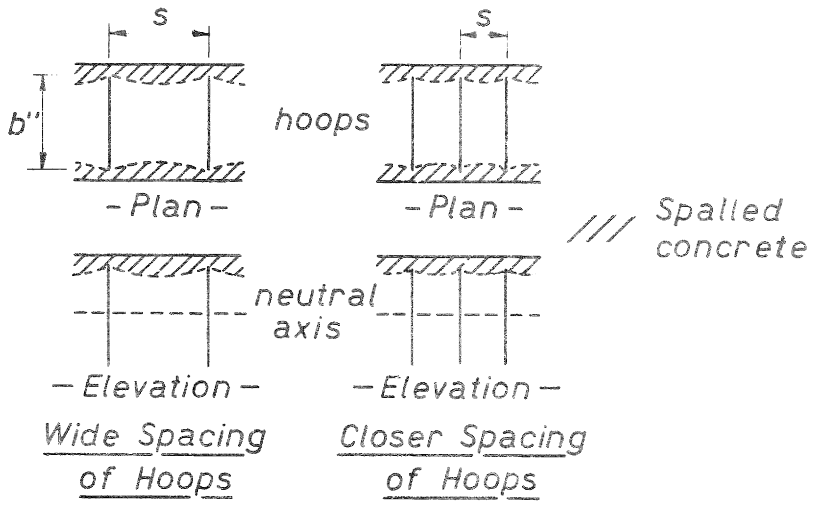

Fig. 9

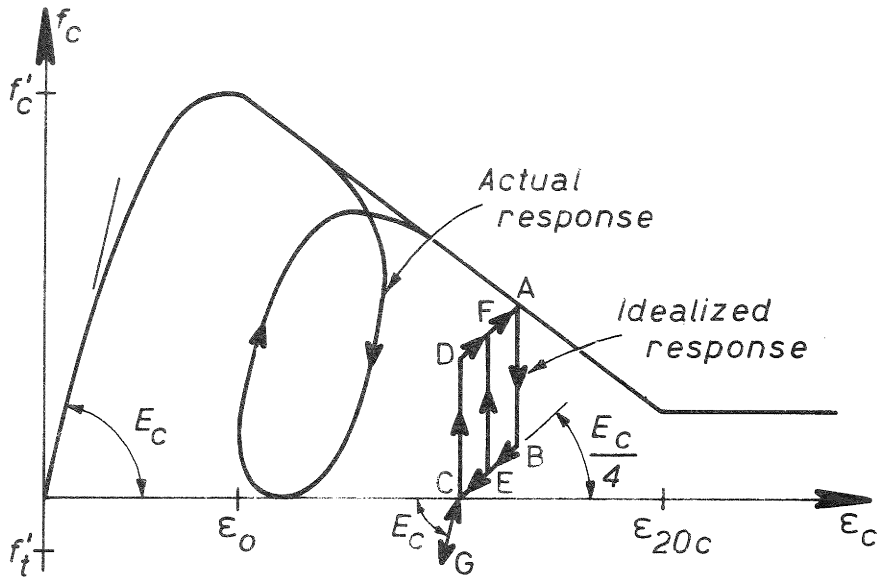
f_c
f'_c
Actual response
Idealized response
A
F
D
B
C
E
E_c
$\frac{E_c}{4}$
ε_o
E_c
G
ε_{20c}
ε_c
f'_t

Fig. 10

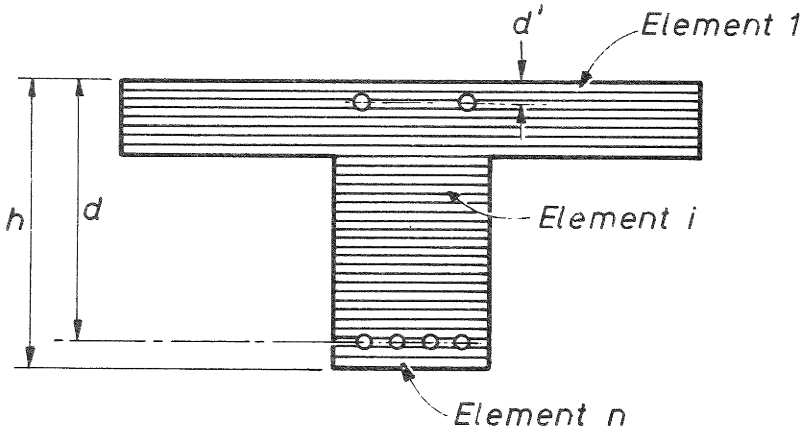
d'
Element 1
h
d
Element i
Element n

Fig. 11

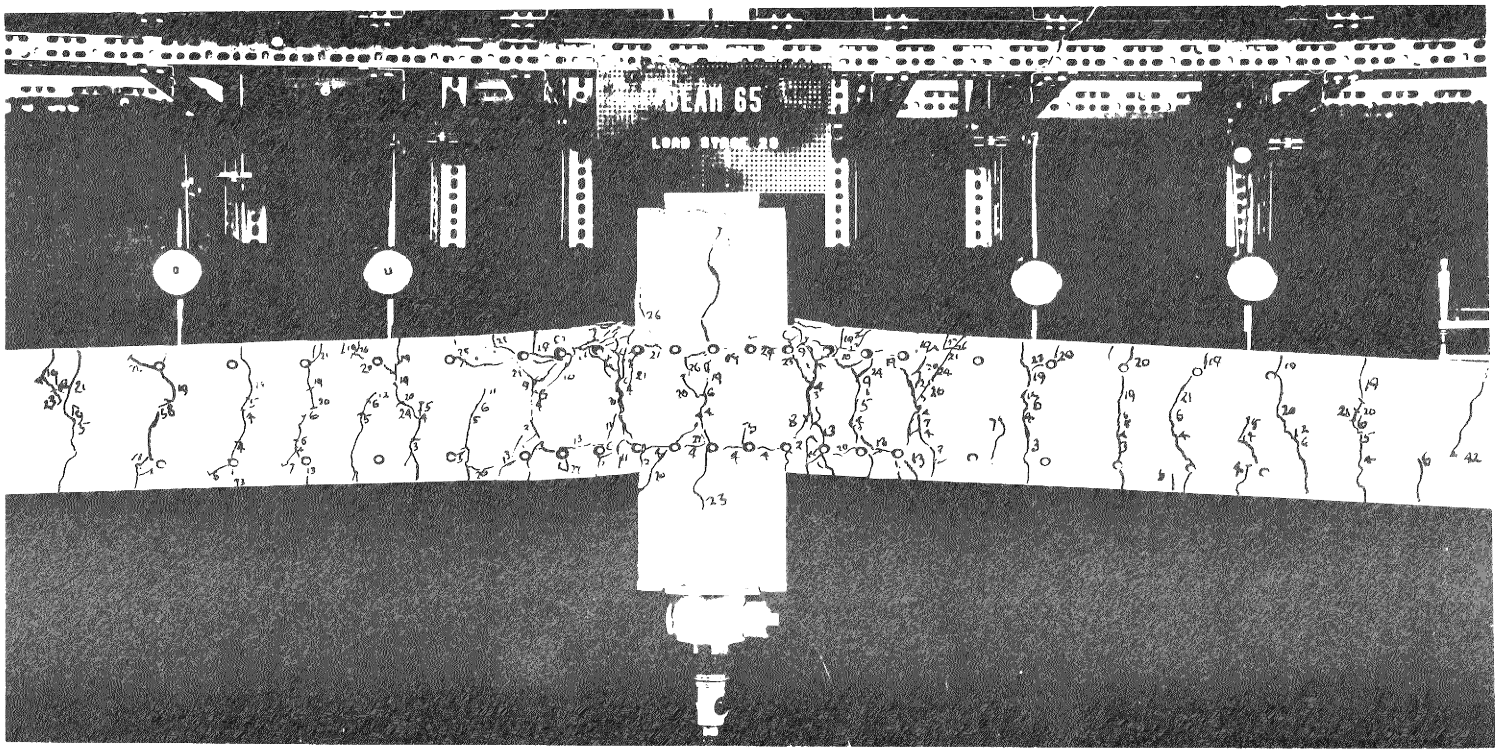

Fig. 12. Beam with p = 1.77%, p′ = 1.12% and p″ = 0.77% After Loading Well Into the Inelastic Range in Each Direction.

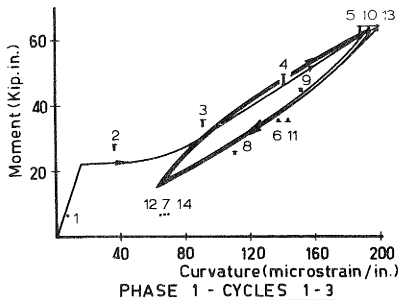

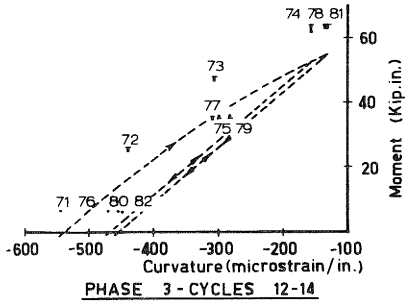

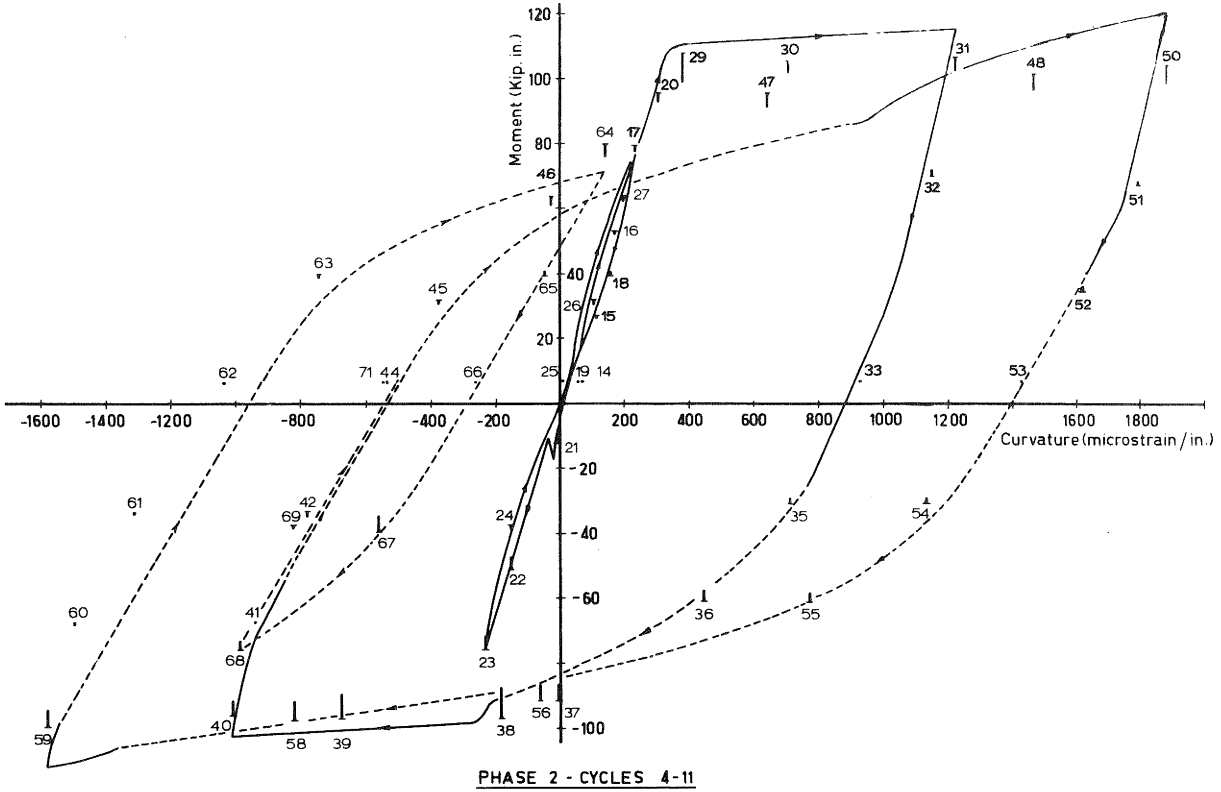

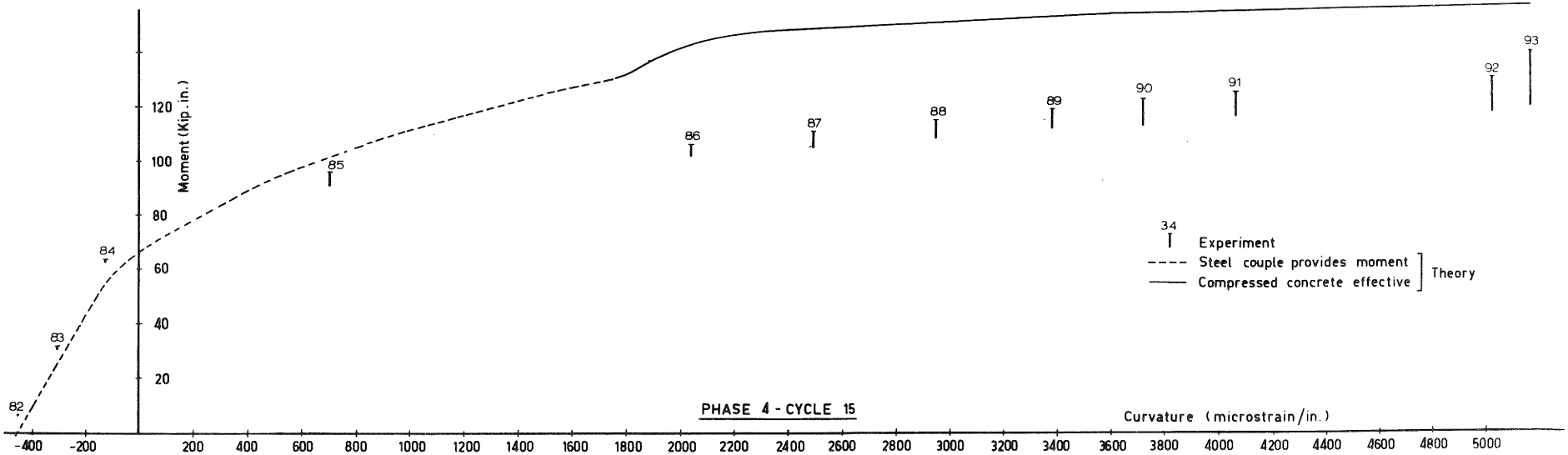

Fig. 13. Moment-Curvature Curves for Critical Section of Beam with p=1.11%, p'=1.11% and p"= 2.30%.

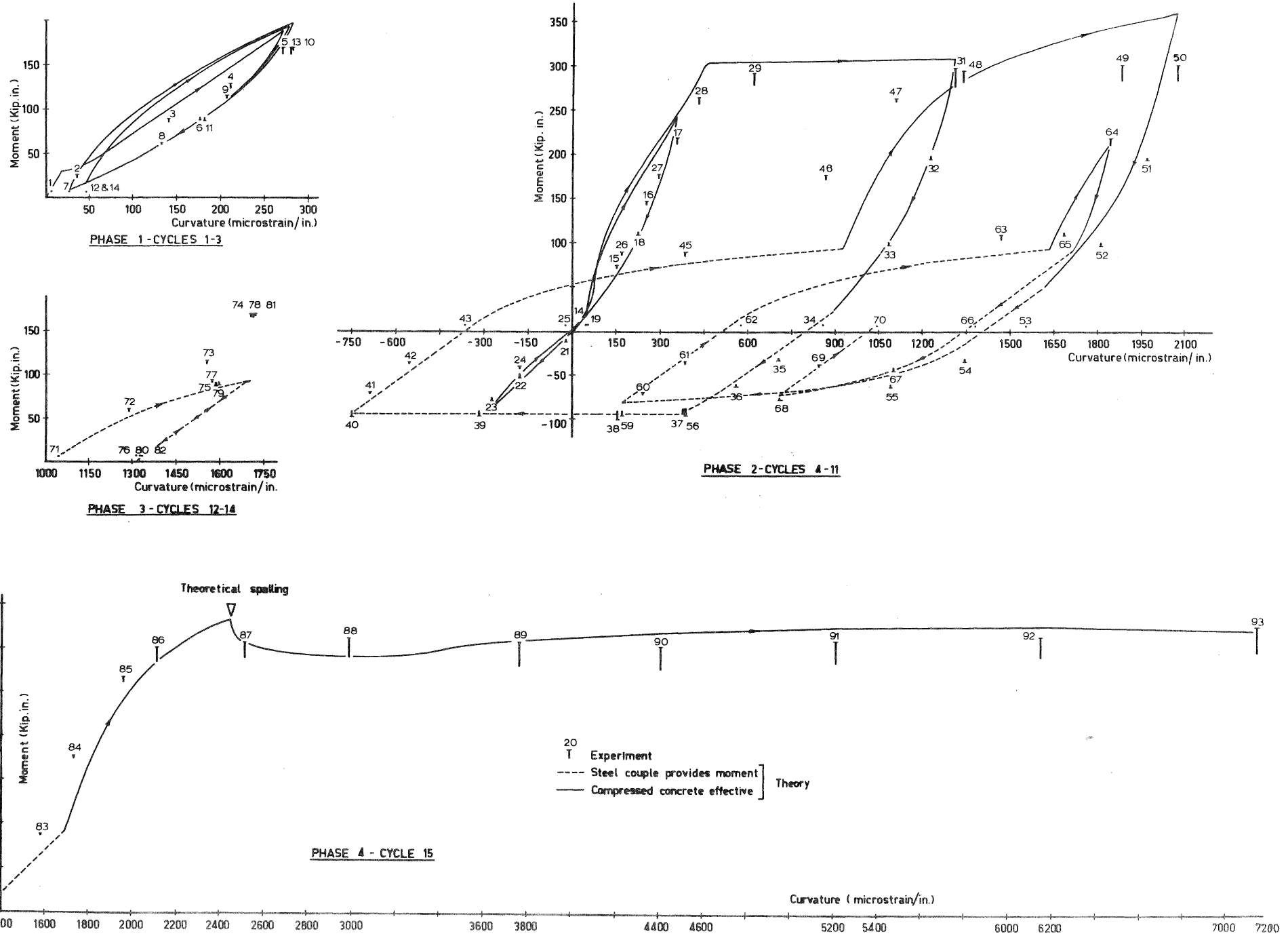

Fig. 14. Moment-Curvature Curves for Critical Section of Beam with p=3.54%, p'=1.14% and p"= 2.30%.

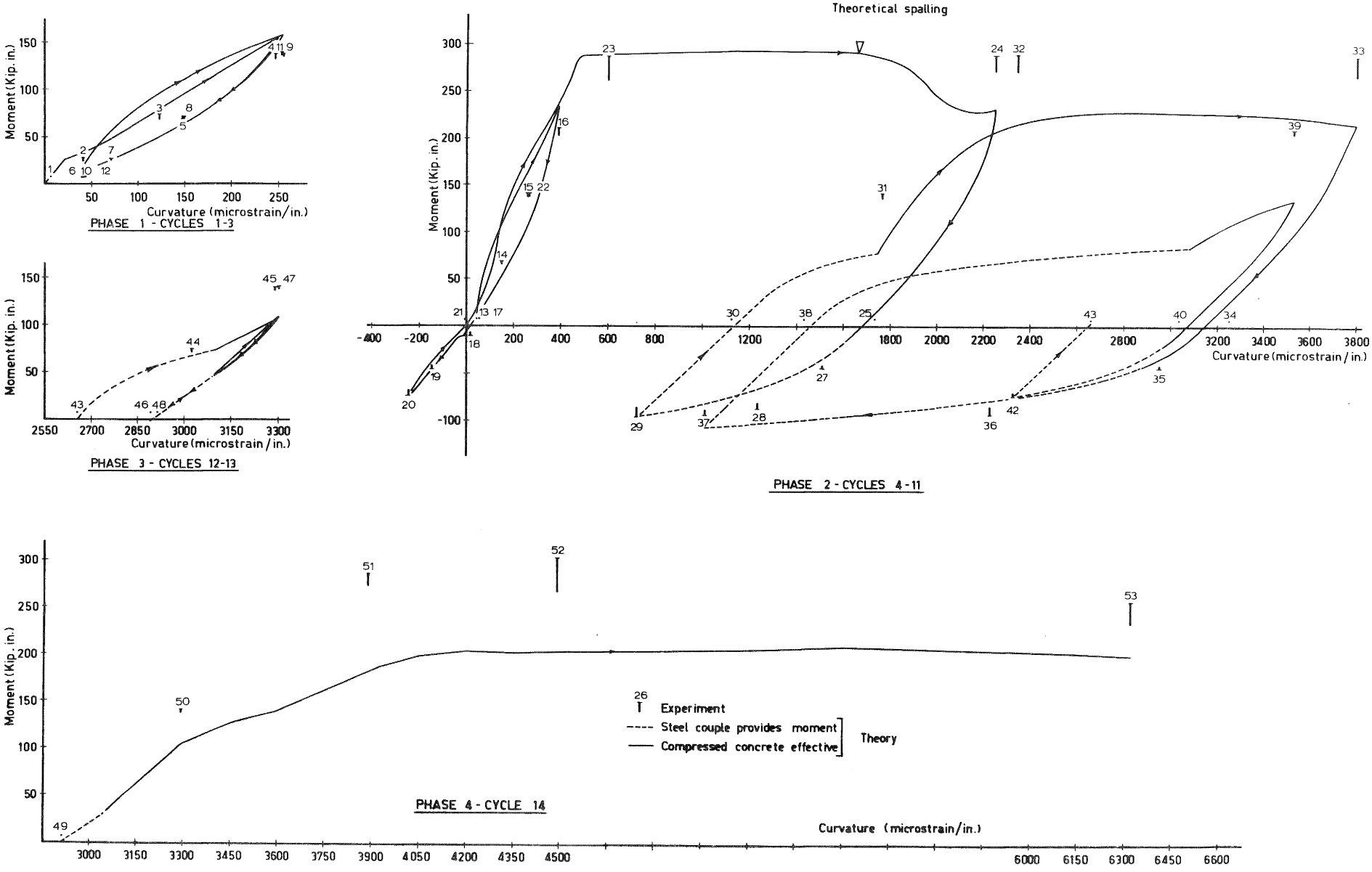

Fig. 15. Moment-Curvature Curves for Critical Section of Beam with $p = 3.54\%$, $p' = 1.14\%$ and $p'' = 0.77\%$.

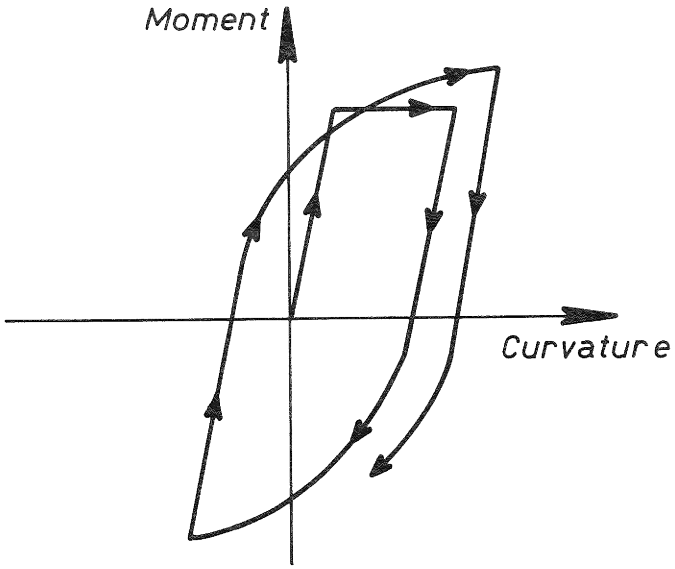

Fig. 16

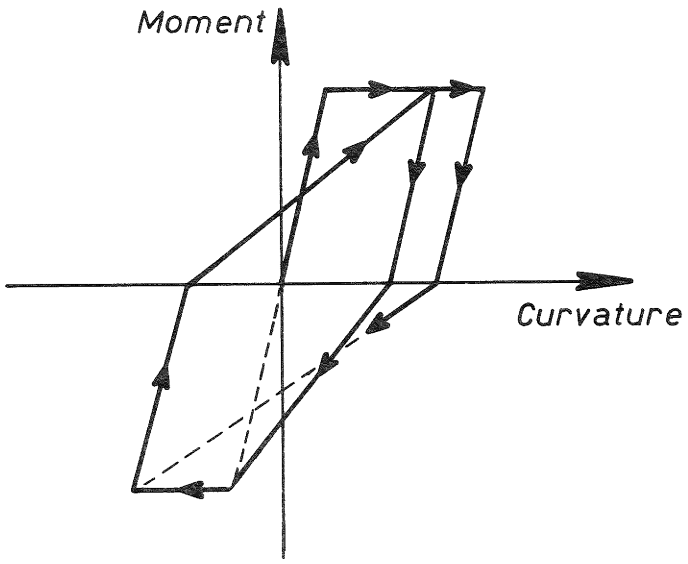

Fig. 17